

Article

# Broadband High-Linear FMCW Light Source Based on Spectral Stitching

Liang Sun <sup>1,2,3</sup>, Xinguang Zhou <sup>4</sup>, Haohao Zhao <sup>2,3</sup>, Shichang Xu <sup>2,3</sup>, Zihan Wu <sup>2,3</sup>, Guohui Yuan <sup>2,3</sup> and Zhuoran Wang <sup>2,3,\*</sup> 

<sup>1</sup> College of Electrical and Information Engineering, Quzhou University, Quzhou 324000, China; 202152011915@std.uestc.edu.cn

<sup>2</sup> Yangtze Delta Region Institute (Quzhou), University of Electronic Science and Technology of China, Quzhou 324003, China; 201811012023@std.uestc.edu.cn (H.Z.); xsc@csj.uestc.edu.cn (S.X.); 202121011423@std.uestc.edu.cn (Z.W.); yuanguohui@uestc.edu.cn (G.Y.)

<sup>3</sup> College of Information and Communication Engineering, University of Electronic Science and Technology of China, Chengdu 610054, China

<sup>4</sup> Zhe Jiang Qi Chao Cable Co., Ltd., Quzhou 324000, China; zxcg197411293116@163.com

\* Correspondence: wangzhuoran@uestc.edu.cn

**Abstract:** The key to realizing a high-performance frequency-modulated continuous wave (FMCW) laser frequency-sweeping light source is how to extend the frequency-swept bandwidth and eliminate the effect of nonlinearity. To solve these issues, this paper designs a broadband high-linear FMCW frequency-sweeping light source system based on the combination of fixed temperature control and digital optoelectronic phase-locked loop (PLL), which controls the temperatures of the two lasers separately and attempts to achieve the coarse spectral stitching based on a time-division multiplexing scheme. Furthermore, we use the PLL to correct the frequency error more specifically after the coarse stitching, which achieves the spectrum fine stitching and, meanwhile, realizes the nonlinearity correction. The experimental results show that our scheme can successfully achieve bandwidth expansion and nonlinearity correction, and the sweeping bandwidth is twice as much as that of the original single laser. The full-width half-maximum (FWHM) of the FMCW output is reduced from 150 kHz to 6.1 kHz, which exhibits excellent nonlinear correction performance. The relative error of the FMCW ranging system based on this frequency-swept light source is also reduced from 1.628% to 0.673%. Therefore, our frequency-swept light source with excellent performance has a promising application in the FMCW laser ranging system.



**Citation:** Sun, L.; Zhou, X.; Zhao, H.; Xu, S.; Wu, Z.; Yuan, G.; Wang, Z.

Broadband High-Linear FMCW Light Source Based on Spectral Stitching.

*Photonics* **2024**, *11*, 477. <https://doi.org/10.3390/photonics11050477>

Received: 13 April 2024

Revised: 12 May 2024

Accepted: 15 May 2024

Published: 19 May 2024



**Copyright:** © 2024 by the authors. Licensee MDPI, Basel, Switzerland. This article is an open access article distributed under the terms and conditions of the Creative Commons Attribution (CC BY) license (<https://creativecommons.org/licenses/by/4.0/>).

**Keywords:** laser ranging; frequency modulated continuous wave; scanning bandwidth expansion; phase-locked loop

## 1. Introduction

Lasers, known for their exceptional collimation and coherence, enable direct measurement of length and displacement. They offer significant advantages in terms of measurement range, accuracy, and speed. In recent years, lasers have been increasingly integrated into the fields of vehicle-mounted airborne radar [1,2], environmental detection [3,4], celestial body detection [5–8], and medical sensing [9,10], to name a few. Currently, laser ranging methods encompass pulse ranging, phase ranging, triangulation ranging, incremental and absolute interference ranging, and frequency modulated continuous wave (FMCW) ranging. The FMCW laser ranging technique has been widely studied by domestic and foreign scholars [11–13] because of its unique advantages such as high adaptability to the measurement environment, robust resistance to noise and interference, advanced automation capabilities, and relatively low complexity.

The frequency-swept light source is the core of the FMCW system, but several key technical challenges remain to be addressed, such as how to correct the light source nonlinearity and how to improve the swept bandwidth. Both issues are closely related to the

performance of the FMCW ranging system. The high-linear swept light source ensures the accuracy of the ranging system, while the swept bandwidth directly affects the measurement resolution. Common realizations for achieving broadband frequency-swept light sources are categorized into external modulation methods [14–18] and internal modulation methods [19,20].

External modulation methods include two coherent optical frequency combs [11], the recirculation frequency shifting technique [15,16], and a single optical frequency comb with dispersion elements [17,18], which require external devices or circuits to achieve a broadband light source. For instance, Yin et al. leveraged optical frequency combs with different spectral ranges to synthesize five narrow-band signals into a 5 GHz broadband signal, and achieved phase stabilization by polarization-multiplexed photoelectronic modulators for the optical frequency comb modulation [14]. Yin et al. used a frequency-shifted cyclic optoelectronic loop for spectral stitching through feedback modulation to generate a broadband linear frequency modulation signal after multiple re-circulations [15], effectively increasing the bandwidth from the original 2 GHz to 3 GHz. Furthermore, Wang et al. proposed a tunable linear frequency modulation signal generation scheme using an optical frequency comb and a fiber Bragg grating time-delay line [17]. By generating multiple spectral lines with the optical frequency comb and separating them with a fiber Bragg grating, they were able to stitch together an optical signal with a bandwidth of 32 GHz.

Internal modulation methods have achieved bandwidth extension by simultaneously modulating the temperature and current of the laser. These techniques have been successfully demonstrated by various researchers with remarkable results. For example, Hefferman et al. simultaneously modulated a single DFB laser with temperature and current and aligned the spectra using cross-correlations [19] to achieve a swept source with a total bandwidth of 510.9 GHz. Li et al. used 10 DFBs with different output wavelengths for spectral concatenation, supplemented by equal optical frequency interval resampling to correct nonlinearity, and successfully increased the resolution of the system by 10 times [20].

In the above work, the implementation of external modulation techniques need to use external devices or external loops such as optical frequency combs, frequency-shifted cyclic photoelectric circuits, and so on. Such requirements add complexity and cost to the design and operation of the light source system. Conversely, the internal modulation method requires a temperature controller that can adjust and stabilize the laser's operating temperature accurately or multiple lasers that can provide adjacent scanning bandwidth, which requires high requirements for device selection.

In this paper, in order to circumvent the issues mentioned above and to realize a broadband high-linear FMCW frequency-sweeping light source system, a bandwidth expansion method based on a coarse temperature control and optoelectronic digital phase-locked loop (PLL) is proposed, and the PLL also offers the function of nonlinear correction of the light source.

## 2. Materials and Methods

### 2.1. FMCW Laser Ranging Method

The FMCW laser ranging system [21] consists of a tunable laser, an interferometer, a spatial light module, and a photodetector (PD), as shown in Figure 1. The system operates by modulating the frequency of the FMCW laser light source. This modulated light then passes through a coupler, which splits the beam into the reference and measurement paths. The light from the measurement path is reflected by the target and then interferes with the light from the reference path to produce the beat frequency signal. The frequency of the beat frequency signal can be extracted and then inverted to the measured distance.

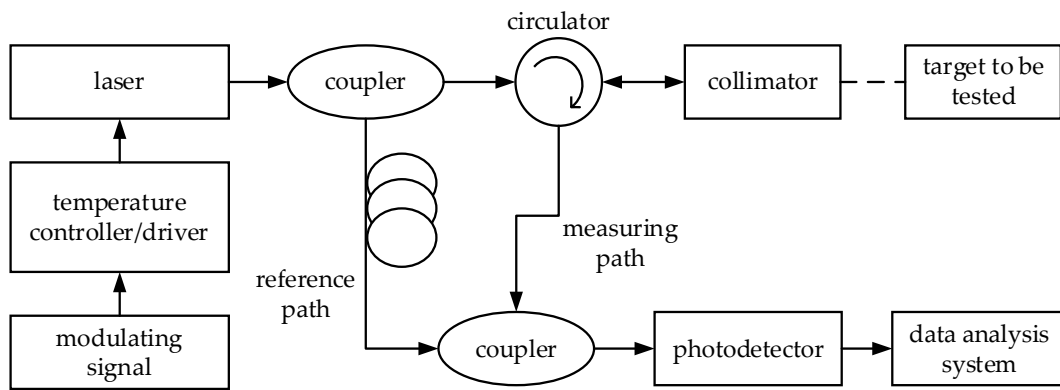


Figure 1. Experimental system structure diagram.

Ideally, the frequencies of the reference beam, the measurement beam, and the beat frequency signal in one modulation cycle are shown in Figure 2, where  $f_1$  is the frequency of the reference signal,  $f_2$  is the frequency of the measured signal,  $f_3$  is the frequency of the beat frequency signal,  $B$  is the sweep bandwidth,  $T$  is the modulation period,  $\tau$  is the time delay due to the optical range difference between the reference and the measured signal, and  $\Delta f$  is the frequency of the beat frequency signal at steady state.

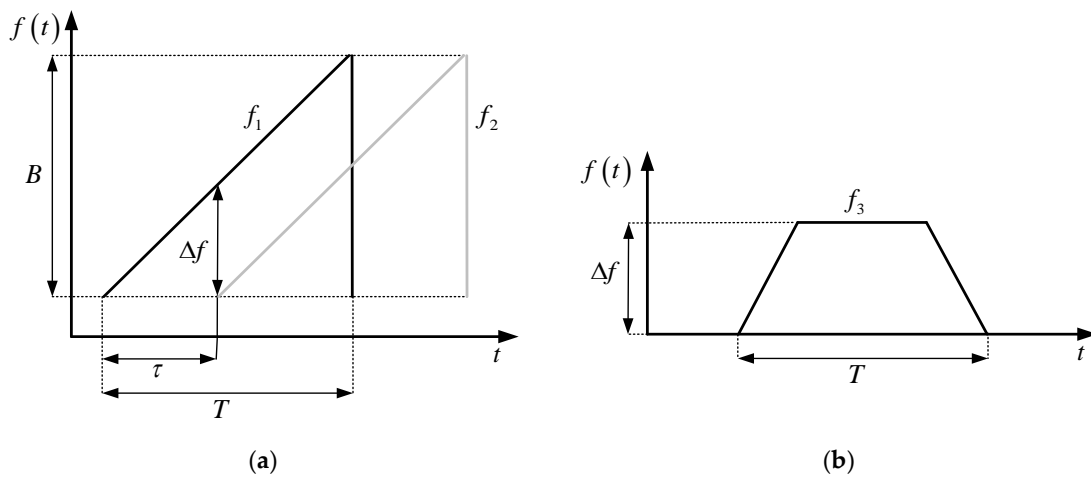


Figure 2. Frequency diagrams of the reference and measurement return beams and beat signals during a single modulation period: (a) frequency diagrams of the reference and measurement return beams; (b) frequency diagram of the beat signal.

The frequency of the beat signal  $\Delta f$  is known from the reference signal and the measured signal:

$$\Delta f = f_1 - f_2 = \frac{B}{T} \tau. \tag{1}$$

$\tau$  can be calculated as follows:

$$\tau = \frac{\Delta d}{v} = \frac{n \Delta d}{c} = \frac{2nd}{c}, \tag{2}$$

where  $\Delta d$  is the optical range difference,  $d$  is the distance of the object to be measured,  $v$  is the speed of light in the medium,  $n$  is the refractive index of the medium, and  $c$  is the speed of light. From the above two equations, the frequency of the beat signal  $\Delta f$  can be obtained as:

$$\Delta f = \frac{2ndB}{Tc}. \tag{3}$$

Therefore,  $\Delta f$  is proportional to the measured distance  $d$ . The inversion leads to the desired measurement distance expression:

$$d = \frac{Tc}{2nB} \Delta f. \tag{4}$$

2.2. Wideband Light Source Implementation Method

The broadband light source system proposed in this paper consists of two tunable lasers, a Mach–Zehnder interferometer (MZI), attenuators, amplifiers, PDs, and FPGA development boards, etc. The system is shown in Figure 3. The FPGA manages time-division multiplexing of the two lasers, which are independently regulated by temperature controllers to operate at different temperatures. These temperatures are carefully selected to facilitate the seamless merging of the lasers’ outputs after injection current modulation, thus contributing to the realization of a broadband light source. The combined output of the two lasers is fed into a coupler to merge the beams. The laser power is then attenuated and the FPGA controls the amplifier to maintain the optimal power level. Finally, the light is subsequently split into three different optical paths by another coupler: one path serves as the output for the ranging system, another is detected with a PD to provide power information for power equalization, and the third path passes through the MZI before being detected with another PD, which provides the frequency for the FPGA to perform nonlinear corrections.

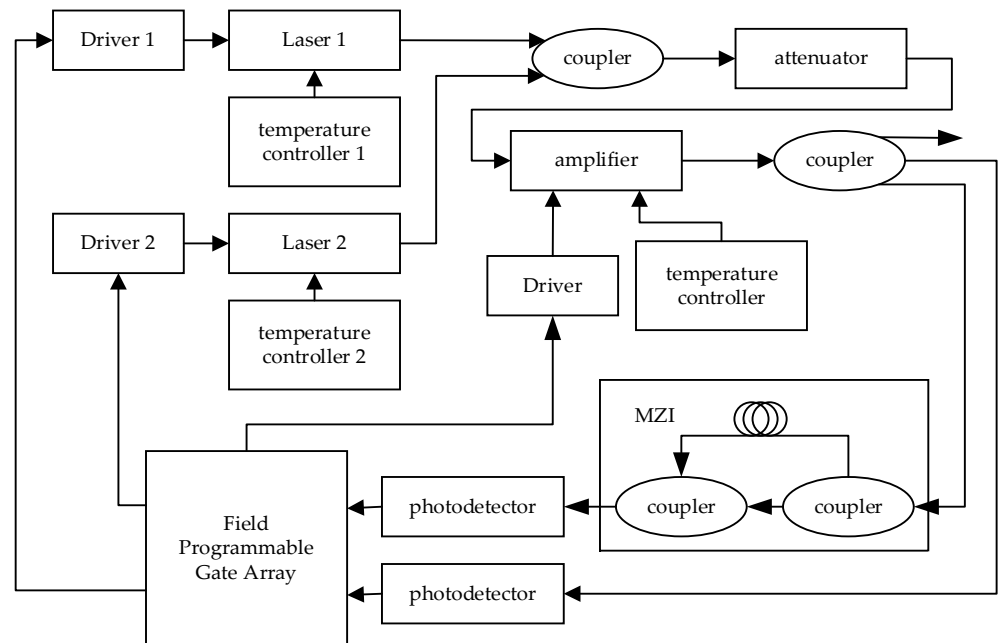
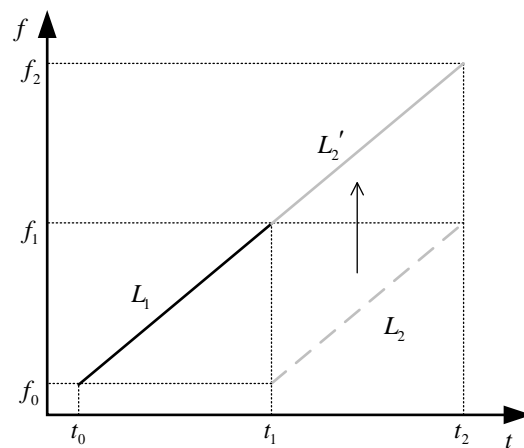


Figure 3. Sweep bandwidth expansion system.

The entire broadband light source system is controlled by four processes: spectral stitching, pre-correction iterative algorithm, power equalization and PLL control.

2.2.1. Spectral Stitching

In this paper, a time division multiplexing scheme is used to achieve spectral stitching to complete the expansion of the FMCW bandwidth. Figure 4 shows the schematic diagram of the implementation of the spectral stitching process.



**Figure 4.** The illustration of spectrum stitching.

When the two lasers work in time-division multiplexing, the FPGA can control the two lasers in the  $t_0 \sim t_1$  and  $t_1 \sim t_2$  time slots, respectively, to complete the frequency sweeping. Meanwhile, if the two lasers have the same operating temperature and modulation signal, the same frequency sweep ranges  $L_1$  and  $L_2$  (dotted line) of the two lasers can be obtained. To achieve the purpose of broadening the bandwidth by stitching their spectra, it is necessary to control the operating temperature of the second laser and the principle is that its initial modulation frequency is set to the maximum modulation frequency of the first laser. Therefore, the two frequencies would be close within a small range due to the presence of the laser noise and frequency drift. This coarse stitching is the basis for the subsequent fine spectral stitching based on PLL control.

### 2.2.2. Pre-Correction Iterative Algorithm

The pre-correction iterative algorithm is used to coarsely linearize the FMCW laser source, laying the foundation for the subsequent digital optoelectronic PLL to stably control the laser’s nonlinearity. In references [22] and [23], it has been discussed how to use iterative algorithms for nonlinear correction. We can derive the iterative formula:

$$\frac{dU_d(t)}{dt} = \frac{\Delta f_d}{\Delta f_0} \cdot \frac{dU_0(t)}{dt}. \tag{5}$$

According to the above iterative formula, we can input the ideal beat frequency signal, the instantaneous frequency of the beat signal, and the modulation voltage at that particular moment. By doing so, the corrected modulation voltage can be derived. By consistently applying this iterative method, the modulation electrical signal can be continuously refined, which enables the achievement of real-time non-linear pre-correction throughout the laser’s operation.

### 2.2.3. Power Equalization

The stable output power of the laser is crucial for the stable control of the subsequent digital optoelectronic PLL. If the power fluctuates greatly, the frequency of the square wave signal converted from the beat frequency signal in the PLL is in error, which has a huge impact on the PLL correction function. The principle of power equalization is as follows.

The optical power equalized by the amplifier can be expressed as:

$$P_{out}(t) = P_{in}(t) \cdot K(i(t)), \tag{6}$$

where  $P_{out}$  is the amplifier output optical power,  $P_{in}$  is the amplifier input optical power,  $i(t)$  is the control signal provided by the FPGA, and  $K(\cdot)$  is the gain coefficient.

After power equalization by the amplifier, the optical power is stable to the ideal optical power  $P_d$ , therefore we have:

$$P_{out}(t) \equiv P_d. \quad (7)$$

From Equations (6) and (7), the control signal  $i(t)$  provided by the FPGA can be introduced as:

$$i(t) = K^{-1} \left( \frac{P_d}{P_{in}(t)} \right). \quad (8)$$

By substituting the ideal optical power, the real-time optical power and the amplifier gain coefficient into the above formula, the corrected control signal is obtained to achieve power equalization during amplifier operation.

#### 2.2.4. Phase-Locked Loop

As mentioned in Section 2.2.2, the operating temperature of the laser can vary and drift during the spectral stitching process. These variations compromise the seamless continuity of the output optical frequency between the two lasers, leading to the emergence of frequency and phase errors. Such discrepancies can be attributed to the nonlinearity introduced during the spectral stitching process.

To address this issue, we propose a PLL method. Utilizing an FPGA as the core processor, we handle the beat frequency signal obtained from the MZI and implement a PLL nonlinearity correction algorithm. The aim of this approach is to correct errors that occur at the stitching junction and to correct the nonlinear distortions inherent in the light source.

The PLL needs to first convert the received beat frequency signal into a square wave signal using the over-zero comparator. The converted square wave signal is phase-discriminated with a reference square wave signal generated by the FPGA itself to produce an error signal. Integration of the error signal provides an adjustment for the modulation current of the laser. This signal is then fed into the laser driver module, enabling the achievement of both fine spectral stitching and sweep nonlinearity correction throughout the operation of the laser.

To handle the large residual error, considering the phase error, external noise, and other factors, this paper designs a PLL with 25 kHz loop bandwidth, 55° phase margin, and 500 kHz reference signal, which enables the PLL to have a large holding range. The narrower loop bandwidth ensures that the PLL can lock to the desired frequency even if residual errors exist. The phase margin setting ensures system stability. The sufficiently large holdover range allows the spectrum to remain within the holdover range when nonlinear errors are outside the loop's capture range, and the PLL remains locked when the initial frequency difference is small.

### 3. Results and Discussion

Concerning that a single-laser based FMCW optical source is the basis of frequency stitching operations for broadband FMCW lasers, we investigate the single-laser experiment to optimize the output performance.

#### 3.1. Single-Laser Experiment

Considering the response time of FPGA, drivers, and lasers, taking into account the ranging range and accuracy of the ranging system, the modulation frequency is set to 1 ms in the experiment. Since the total length of the fibers in the MZI used does not exceed 3 m and the fiber dispersion is small, the experiment does not take into account the fiber dispersion contained in the MZI. And we utilize a 1550 nm tunable DFB with a sweep bandwidth of approximately 80 GHz to accomplish the experiments on power equalization and nonlinearity correction. The optical power level is reflected in the envelope signal collected with the PD, and the envelope signals, both before and after power equalization, are shown in Figure 5. After power equalization, the amplitude of the envelope signal

is significantly reduced from 1.18 V to less than 0.1 V. This result proves that the power equalization can effectively stabilize the power.

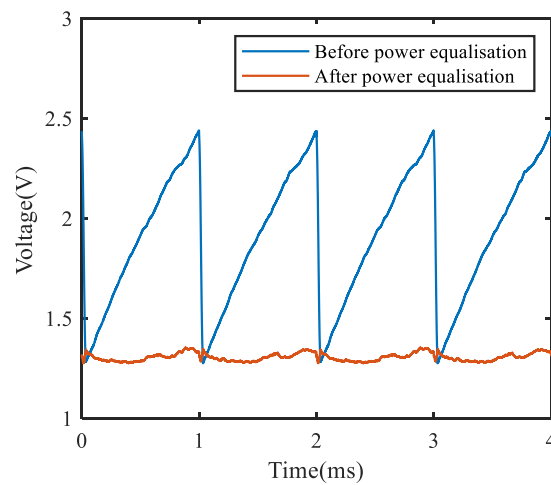


Figure 5. Envelope signal plots before and after power equalization.

The residual error graph and sweep frequency graph [18], both before and after the application of the nonlinear correction, are shown in Figure 6.

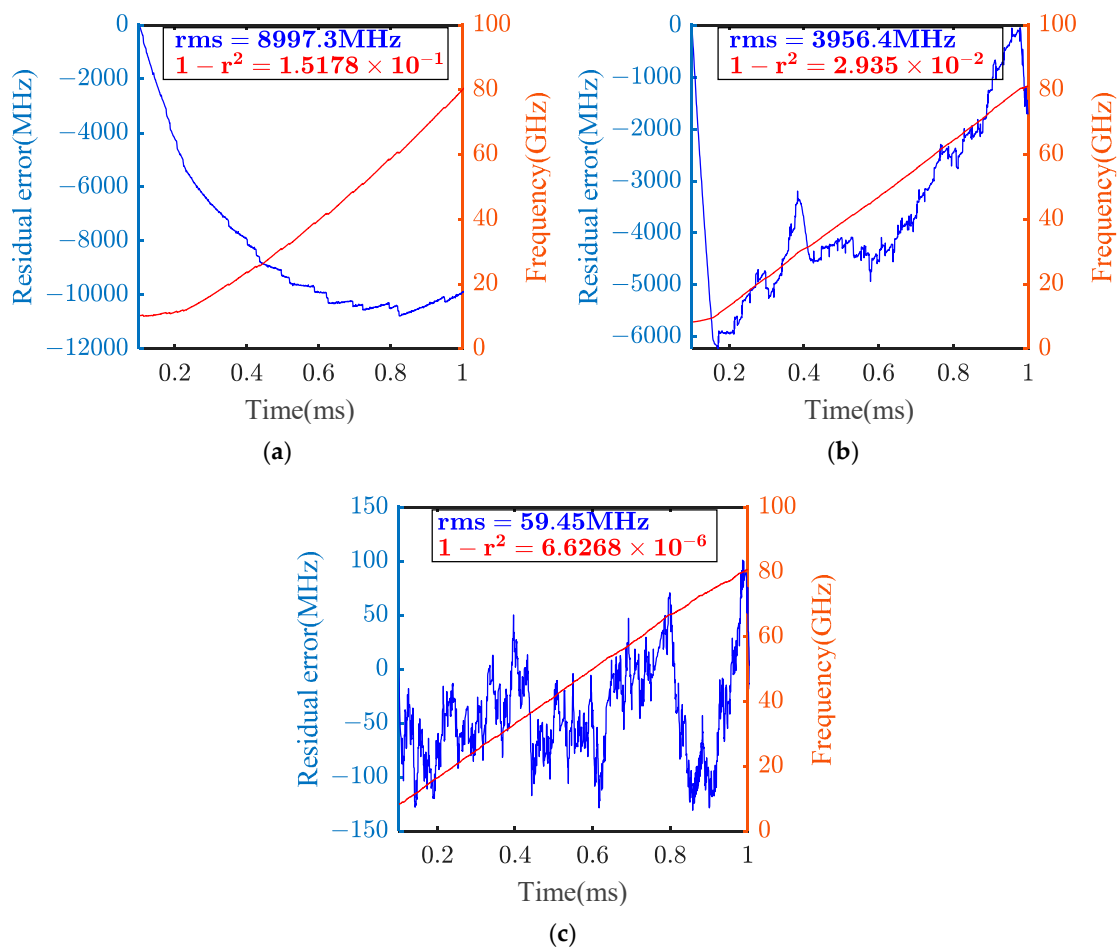
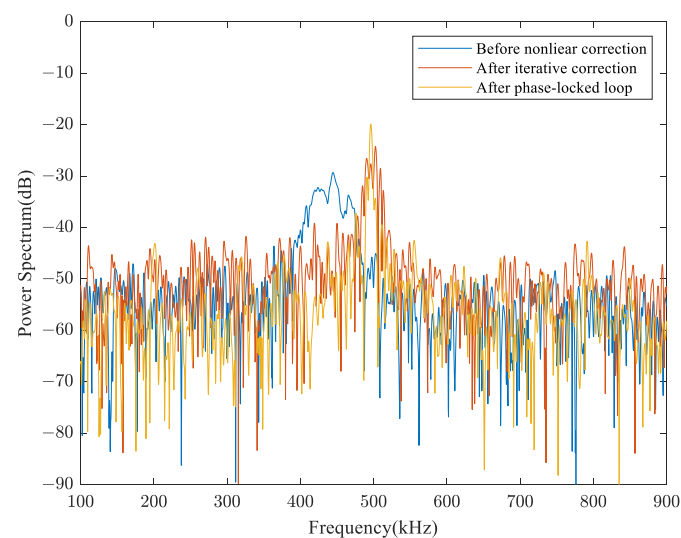


Figure 6. Residual error graph and sweep frequency graph: (a) before nonlinear correction; (b) after iterative algorithm correction; and (c) after phase-locked loop.

As illustrated in the figure, the red curve represents the actual optical output frequency over time for a single cycle, while the blue curve denotes the difference between the actual optical frequency and the ideal swept frequency. The comparison reveals that there is a residual nonlinearity of 9 GHz in the absence of nonlinear correction, with  $1 - r^2$  of  $1.5 \times 10^{-1}$ . Following the application of the iterative algorithm correction, the residual nonlinearity is reduced to 4 GHz, and  $1 - r^2$  is reduced to  $2.9 \times 10^{-2}$ , indicating a slight improvement in the performance.

Further refinement using phase-locking reduces the residual nonlinearity to 59.5 MHz and  $1 - r^2$  to  $6.6 \times 10^{-6}$ , with a significant improvement in performance. The spectrograms of the beat-frequency signals are shown in Figure 7. Prior to nonlinear correction, the peak of the beat-frequency signal spectrum appears to be considerably broader, with the full-width half-maximum (FWHM) of 87.1 kHz. After the iterative algorithm correction, the FWHM of the beat-frequency signal spectrum narrows to 7.9 kHz. Finally, the FWHM is further refined to 4.1 kHz with additional phase-locking through PLLs.



**Figure 7.** Spectrum diagrams of beat frequency signals.

Therefore, the single-laser light source system equipped with iterative algorithms and digital PLL corrections can effectively reduce the nonlinear effects, resulting in an excellent FMCW laser light source.

### 3.2. Bandwidth Expansion Experiment

Based on the single-laser system in the previous section, two 1550 nm tunable DFBs are used in this section to perform the bandwidth expansion experiments. These experiments maintain the same parameters, with a sweep period of 1 ms and a sweep bandwidth of approximately 80 GHz. Subsequently, an in-depth comparison is carried out, which includes analyzing the spectrum of the swept light source, the beat frequency signal spectrum, the residual nonlinear error curve of the output signal, and the frequency-swept diagrams both before and after the bandwidth expansion. The purpose of this comparison is to highlight the advantages and limitations of the light source in both its pre-expanded and post-expanded bandwidth states.

The experimental setup of the spectrograph RBW is 0.1 nm and VBW is 1 kHz, and the spectra before and after bandwidth expansion are shown in Figure 8. This figure demonstrates the ability of a single laser to offer a sweep bandwidth of about 80 GHz, with a sweep range extending from 193.67 THz to 193.75 THz. Subsequently, by fine-tuning the operating temperature of the second laser, the coarse spectral stitching is achieved. This adjustment enables the second laser to provide a sweep bandwidth of approximately 80 GHz, with a sweep range of 193.59 THz to 193.67 THz.

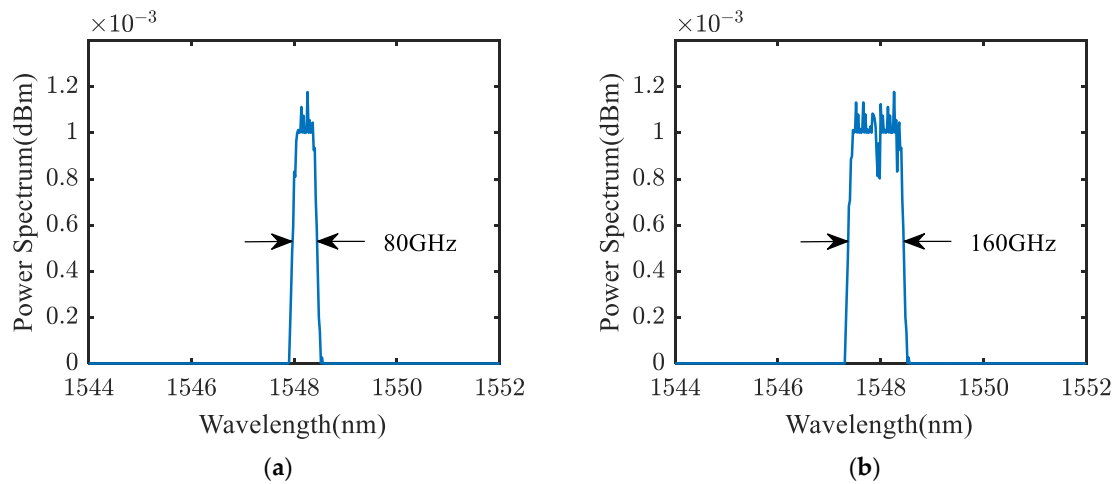


**Figure 8.** Sweep frequency spectrum: (a) before expanding the sweep bandwidth; (b) after expanding the sweep bandwidth.

By implementing time-division multiplexing control of the light source and then optically combining the output beams of the two lasers via a coupler, a broadband frequency-sweeping light source with an extended bandwidth of approximately 160 GHz is realized. This approach effectively broadens the frequency sweep range from 193.59 THz to 193.75 THz.

However, after the above coarse spectral stitching is completed, there are still frequency discontinuities and phase errors at the stitching junction. This will affect the performance of the broadband light source, resulting in high nonlinear errors in the second half of the cycle, as shown in Figure 9a at 0.5 ms. In order to reduce the nonlinear error generated by stitching operation, a PLL is introduced to phase-lock the two lasers, and the resulting residual nonlinear curves and sweep plots are shown in Figure 9b.

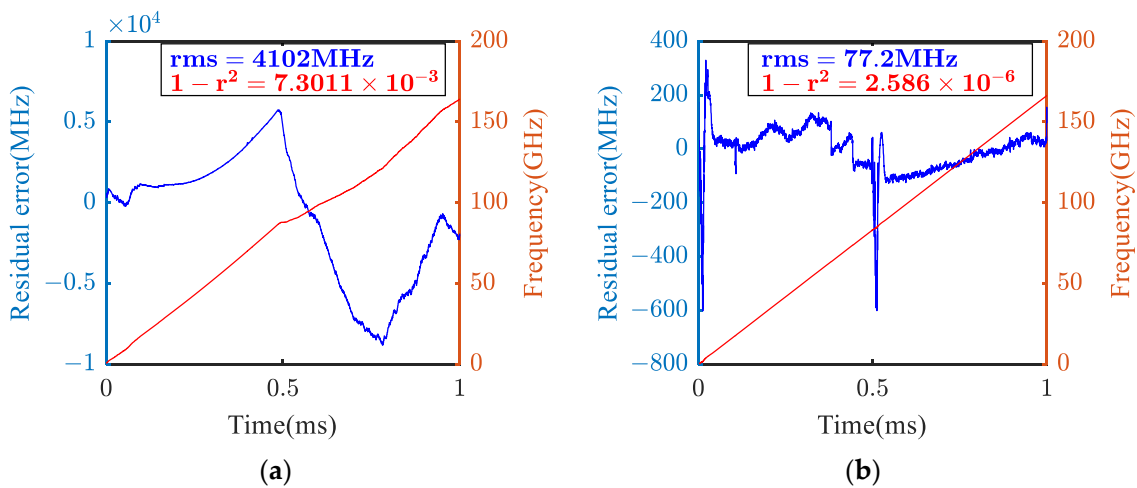


**Figure 9.** Residual error graph and sweep frequency graph: (a) before expanding the sweep bandwidth; (b) after expanding the sweep bandwidth.

As can be seen from the comparison in Figure 9, after PLL locking, the portion of the high nonlinearity generated at 0.5 ms in Figure 9a quickly returns to the desired frequency in Figure 9b, with a minimal frequency fluctuation lasting only 0.03 ms. Without phase locking, a residual nonlinearity of 4.1 GHz exists, with  $1 - r^2$  of  $7.3 \times 10^{-3}$ . After the phase locking, the residual nonlinearity is reduced to 77.2 MHz, and  $1 - r^2$  is reduced to  $2.6 \times 10^{-6}$ . Before locking, the spectrum of the beat frequency signal exhibits a noticeable spread in Figure 10, with a FWHM of 150 kHz. However, after PLL locking, the FWHM

of the beat frequency signal spectrum narrows to 6.1 kHz. This refinement in spectral resolution demonstrates the effectiveness of the phase-locking technique in improving the laser ranging system's performance.

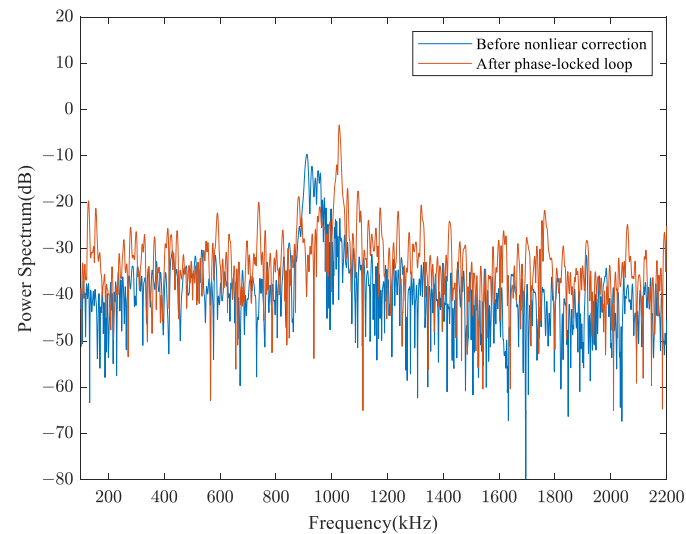


**Figure 10.** Spectra of beat frequency signals.

Therefore, our proposed dual-laser light source system, which employs temperature control, time-division multiplexing, and digital PLL corrections, is capable of achieving a significantly expanded swept bandwidth while effectively suppressing the nonlinearities of the lasers.

### 3.3. Distance Measuring Experiment

Ranging experiments based on the proposed light source system have been conducted to evaluate the performance. The accuracy of the ranging measurements is confirmed through the assessment of relative distances, both prior to and following any displacement, as depicted in the spectrogram of the beat-frequency signal presented in Figure 11.

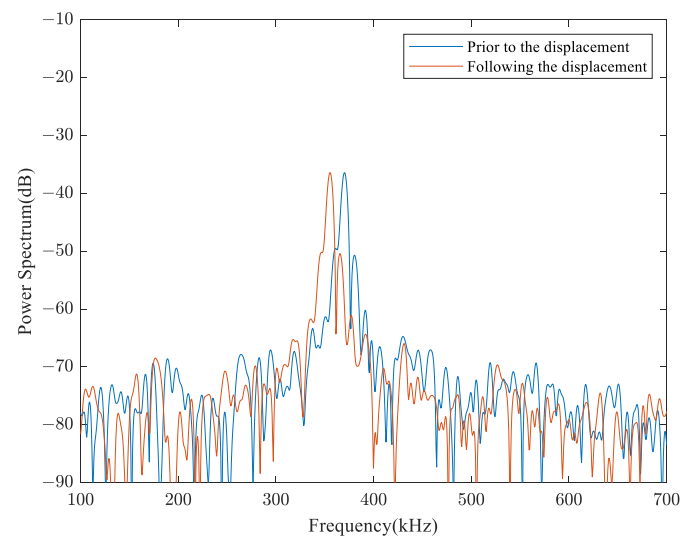


**Figure 11.** Spectra of beat frequency signals prior to and following the displacement.

A set of frequency differences can be obtained from the spectrograms of the spectral signals before and after displacement, and the corresponding distance values can be obtained by substituting the frequency differences into Equation (4). Six positions on the

displacement platform are selected for measurement, each position corresponding to a displacement of 20 mm. The results of the distance measurements, both before and after the expansion of the sweep bandwidth, are presented in Table 1.

**Table 1.** Analysis table of distance measurement results.

Experimental Stage	Before Extending the Sweep Bandwidth $d_1/\text{mm}$	After Extending the Sweep Bandwidth $d_2/\text{mm}$
1	19.903	19.898
2	19.329	19.953
3	20.531	19.743
4	20.237	20.245
5	20.332	20.116
6	20.261	20.042
average error	0.01628	0.00673

As depicted in Table 1, the ranging accuracy is enhanced to the sub-millimeter level after the expansion of the swept bandwidth. The average errors recorded before and after the bandwidth expansion are 1.628% and 0.673%, respectively, representing a decrease of approximately 50%. The results confirm that the dual-laser light source system is capable of achieving enhanced ranging accuracy.

Afterwards, the distance resolution of the ranging system is also investigated. Figure 12 shows the spectra of the received signals when measuring a 1.94 mm acrylic plate before and after the swept bandwidth expansion. As the acrylic plate used for the experiment has no permeable or anti-transparent membrane, the resonance is generated within the acrylic plate, causing the periodic oscillation in the spectrum.

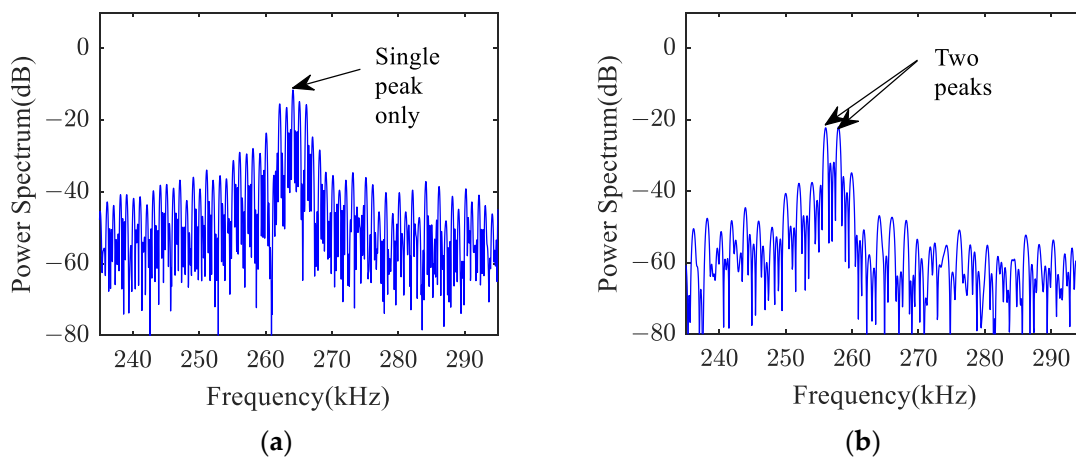


**Figure 12.** Spectrum diagrams of received signal: (a) before expanding the sweep bandwidth; (b) after expanding the sweep bandwidth.

Prior to bandwidth expansion, the spectrum of the received signal is unable to resolve the two spectral peaks from the reflective surfaces of the transparent acrylic plate. However, after bandwidth expansion, the received signal spectrum clearly exhibits two distinct spectral peaks, enabling the effective thickness measurement of the transparent acrylic plate. The measured thickness is determined to be 1.8 mm, which corresponds to a relative error of 0.14 mm when compared to the actual thickness of 1.94 mm. This result demonstrates the broadband light source system’s ability in measuring smaller distances with consistent sub-millimeter accuracy.

Consequently, the dual-laser light source system, equipped with temperature control, time-division multiplexing, and digital PLL correction for swept-bandwidth expansion,

has demonstrated its ability to achieve enhanced distance resolution. This technological advance is critical for applications requiring high-precision distance measurements, particularly in scenarios involving small dimensions or complex geometries.

#### 4. Conclusions

In this paper, dual DFBs are used as the frequency-swept light source for the FMCW laser ranging system. By employing temperature control and time division multiplexing, the coarse spectral stitching was successfully performed. Subsequently, the implementation of a digital PLL facilitated fine spectrum stitching and accomplished the nonlinear correction of the lasers, which finally achieved the purpose of linearization of the frequency-sweeping light source while increasing the sweeping bandwidth of the light source. The results indicated that the sweeping bandwidth of the light source has been extended from 80 GHz to 160 GHz, and the FWHM of the beat signal remains consistently at 6.1 kHz, and the range error can be reduced by 50% compared to pre-bandwidth expansion levels. This bandwidth expansion technique is straightforward to implement, and the nonlinear correction performance is excellent. The concepts presented in this paper can be applied to scale up the system by increasing the number of DFBs to four, eight, or even sixteen channels, which could further broaden the sweep bandwidth. Such an approach holds significant potential for advancing the development of high-performance laser ranging systems, offering improved accuracy and reliability in various applications.

**Author Contributions:** L.S. completed the experiment and wrote the manuscript; H.Z., X.Z. and S.X. conduct relevant literature search and conduct feasibility analysis; Z.W. (Zihan Wu) wrote part of the code; G.Y. and Z.W. (Zhuoran Wang) proposed the idea, helped to modify the manuscript and supervised the project. All authors have read and agreed to the published version of the manuscript.

**Funding:** This work is financially supported by Zhejiang Provincial National Natural Science Foundation of China (Y23F050001, LZYZ4F050002), partly by Natural Science Foundation of Sichuan, China under Grant Numbers (2023NSFSC0492), partly by Medico-Engineering Cooperation Funds from University of Electronic Science and Technology of China under Grant Number (ZYGX2021YGLH214), partly by the Municipal Government of Quzhou under Grant Numbers (2023D001, 2023D020, 2022D032, 2022D026).

**Institutional Review Board Statement:** Not applicable.

**Informed Consent Statement:** Not applicable.

**Data Availability Statement:** The raw data supporting the conclusions of this article will be made available by the authors on request.

**Conflicts of Interest:** The authors declare no conflicts of interest. Author Xinguang Zhou was employed by the company Zhe Jiang Qi Chao Cable CO., LTD., Quzhou, China. The remaining authors declare that the research was conducted in the absence of any commercial or financial relationships that could be construed as a potential conflict of interest.

#### References

1. Aksarin, S.; Ganin, D.; Feng, C.; Smolovik, M.; Zott, A.; Davydenko, V. Optimizing of laser source parameters for FMCW automotive LiDARs. In Proceedings of the Conference on Photonic Instrumentation Engineering X, San Francisco, CA, USA, 30 January–1 February 2023; SPIE: Washington, DC, USA, 2023; p. 124280X. [\[CrossRef\]](#)
2. Gogoi, T.; Kumar, R. Design and development of a laser warning sensor prototype for airborne application. *Def. Sci. J.* **2023**, *73*, 332–340. [\[CrossRef\]](#)
3. Li, X.Y.; Li, F.Y. Displacement monitoring requirements and laser displacement monitoring technology of bridges with short and medium spans. *Appl. Sci.* **2022**, *12*, 9663. [\[CrossRef\]](#)
4. Wang, B.J.; Guo, Z.W.; Shen, Z.M.; Xu, H.; Liu, L.; Li, J.X. Underwater 3D imaging utilizing 520 nm chaotic lidar. *J. Russ. Laser Res.* **2020**, *41*, 399–405. [\[CrossRef\]](#)
5. Han, X.D.; Wu, X.L.; Zhao, H.C.; Lin, X.D.; Li, M.; Wu, Z.G. Application of optical switching technology in a lunar laser ranging system based on a superconducting detector. *Appl. Opt.* **2023**, *62*, 5348–5354. [\[CrossRef\]](#) [\[PubMed\]](#)
6. Ipatov, A.V.; Vedeshin, L.A. Laser applications in ground-based and space observations (marking 60 years since the first experiments on lunar laser ranging). *Izv. Atmos. Ocean. Phys.* **2021**, *57*, 1794–1796. [\[CrossRef\]](#)

7. Chabe, J.; Courde, C.; Torre, J.M.; Bouquillon, S.; Bourgoïn, A.; Aïmar, M.; Albanese, D.; Chauvineau, B.; Mariey, H.; Martinot-Lagarde, G.; et al. Recent progress in lunar laser ranging at grasse laser ranging station. *Earth Space Sci.* **2019**, *7*, e2019EA000785. [[CrossRef](#)]
8. Meng, W.D.; Zhang, H.F.; Deng, H.R.; Tang, K.; Wu, Z.B.; Wang, Y.R.; Wu, G.; Zhang, Z.P.; Chen, X.Y. 1.06  $\mu\text{m}$  wavelength based high accuracy satellite laser ranging and space debris detection. *Acta Phys. Sin.* **2020**, *69*, 019502. [[CrossRef](#)]
9. Vizbaras, A.; Simonyte, I.; Droz, S.; Torcheboeuf, N.; Miasojedovas, A.; Trinkunas, A.; Buciuinas, T.; Dambrauskas, Z.; Gulbinas, A.; Boiko, D.L.; et al. GaSb swept-wavelength lasers for biomedical sensing applications. *IEEE J. Sel. Top. Quantum Electron.* **2019**, *25*, 1501812. [[CrossRef](#)]
10. Jeff, P.; Logan, C.; Kevin, W. Fiber laser design for biomedical applications. In Proceedings of the Conference on Optical Fibers and Sensors for Medical Diagnostics, Treatment and Environmental Applications XXIII, San Francisco, CA, USA, 28–30 January 2023; SPIE: Washington, DC, USA, 2023; p. 123720C. [[CrossRef](#)]
11. Barber, Z.W.; Babbitt, W.R.; Kaylor, B.; Reibel, R.R.; Roos, P.A. Accuracy of active chirp linearization for broadband frequency modulated continuous wave ladar. *Appl. Opt.* **2010**, *49*, 213–219. [[CrossRef](#)]
12. Pan, H.; Zhang, F.M.; Shi, C.Z.; Qu, X.H. High-precision frequency estimation for frequency modulated continuous wave laser ranging using the multiple signal classification method. *Appl. Opt.* **2017**, *56*, 6956–6961. [[CrossRef](#)] [[PubMed](#)]
13. Qin, J.; Zhang, L.; Xie, W.L.; Cheng, R.; Liu, Z.W.Y.; Wei, W.; Dong, Y. Ultra-long range optical frequency domain reflectometry using a coherence-enhanced highly linear frequency-swept fiber laser source. *Opt. Express* **2019**, *27*, 19359–19368. [[CrossRef](#)]
14. Yin, F.F.; Yin, Z.K.; Xie, X.Z.; Dai, Y.T.; Xu, K. Broadband radio-frequency signal synthesis by photonic-assisted channelization. *Opt. Express* **2021**, *29*, 17839–17848. [[CrossRef](#)] [[PubMed](#)]
15. Yin, Z.Q.; Zhang, X.P.; Liu, C.Y.; Zeng, H.N.; Li, W.Z. Wideband reconfigurable signal generation based on recirculating frequency-shifting using an optoelectronic loop. *Opt. Express* **2021**, *29*, 28643–28651. [[CrossRef](#)]
16. Wen, L.; Wang, Z.Y.; Yuan, Q.; Yang, T.X.; Ge, C.F.; Hu, D.N.; Qin, J.Q. Tunable linear-step-swept light source based on time-delayed spectrum stitching technique. In Proceedings of the Conference on Terahertz, RF, Millimeter, and Submillimeter-Wave Technology and Applications XIII, San Francisco, CA, USA, 3–6 February 2020; SPIE: Washington, DC, USA, 2020; Volume 11279, p. 1127924. [[CrossRef](#)]
17. Wang, X.C.; Ma, J.X.; Zhang, Q.; Xin, X.J. Generation of linear frequency-modulated signals with improved time-bandwidth product based on an optics frequency comb. *Appl. Opt.* **2019**, *58*, 3222–3228. [[CrossRef](#)] [[PubMed](#)]
18. Li, J.D.; Xue, X.X.; Yang, B.F.; Wang, M.A.; Li, S.Y.; Zheng, X.P. Broadband linear frequency-modulated waveform generation based on optical frequency comb assisted spectrum stitching. *Opt. Express* **2022**, *30*, 24145–24154. [[CrossRef](#)] [[PubMed](#)]
19. Hefferman, G.; Chen, Z.; Wei, T. Extended-bandwidth frequency sweeps of a distributed feedback laser using combined injection current and temperature modulation. *Rev. Sci. Instrum.* **2017**, *88*, 075104. [[CrossRef](#)] [[PubMed](#)]
20. Li, C.L.; Zhang, F.M.; Qu, X.H. High-resolution frequency-modulated continuous-wave LiDAR using multiple laser sources simultaneously scanning. *J. Lightw. Technol.* **2023**, *41*, 367–373. [[CrossRef](#)]
21. Zhang, X.B.Q.; Kong, M.; Guo, T.T.; Zhao, J.; Wang, D.D.; Liu, L.; Liu, W.; Xu, X.K. Frequency modulation nonlinear correction and range-extension method based on laser frequency scanning interference. *Appl. Opt.* **2021**, *60*, 3446–3451. [[CrossRef](#)] [[PubMed](#)]
22. Zhang, X.S.; Jazz, P.; Ming, C.W. Laser frequency sweep linearization by iterative learning pre-distortion for FMCW LiDAR. *Opt. Express* **2019**, *27*, 9965–9974. [[CrossRef](#)] [[PubMed](#)]
23. Li, P.; Zhang, Y.T.; Yao, J.Q. Rapid linear frequency swept frequency-modulated continuous wave laser source using iterative pre-distortion algorithm. *Remote Sens.* **2022**, *14*, 3455. [[CrossRef](#)]

**Disclaimer/Publisher’s Note:** The statements, opinions and data contained in all publications are solely those of the individual author(s) and contributor(s) and not of MDPI and/or the editor(s). MDPI and/or the editor(s) disclaim responsibility for any injury to people or property resulting from any ideas, methods, instructions or products referred to in the content.